Structural Analysis of Golgi α-Mannosidase II Inhibitors Identified from a Focused Glycosidase Inhibitor Screen[†,‡]

Douglas A. Kuntz,[§] Chris A. Tarling,[||] Stephen G. Withers,[||] and David R. Rose*[,§,#]

Ontario Cancer Institute and Department of Medical Biophysics, University of Toronto, Toronto, Ontario, Canada, and Department of Chemistry, University of British Columbia, Vancouver, British Columbia, Canada

Received June 6, 2008; Revised Manuscript Received July 28, 2008

ABSTRACT: The N-glycosylation pathway is a target for pharmaceutical intervention in a number of pathological conditions including cancer. Golgi α-mannosidase II (GMII) is the final glycoside hydrolase in the pathway and has been the target for a number of synthetic efforts aimed at providing more selective and effective inhibitors. *Drosophila* GMII (dGMII) has been extensively studied due to the ease of obtaining high resolution structural data, allowing the observation of substrate distortion upon binding and after formation of a trapped covalent reaction intermediate. However, attempts to find new inhibitor leads by high-throughput screening of large commercial libraries or through *in silico* docking were unsuccessful. In this paper we provide a kinetic and structural analysis of five inhibitors derived from a small glycosidase-focused library. Surprisingly, four of these were known inhibitors of *β*-glucosidases. X-ray crystallographic analysis of the dGMII:inhibitor complexes highlights the ability of the zinc-containing GMII active site to deform compounds, even ones designed as conformationally restricted transition-state mimics of *β*-glucosidases, into binding entities that have inhibitory activity. Although these deformed conformations do not appear to be on the expected conformational itinerary of the enzyme, and are thus not transition-state mimics of GMII, they allow positioning of the three vicinal hydroxyls of the bound gluco-inhibitors into similar locations to those found with mannose-containing substrates, underlining the importance of these hydrogen bonds for binding. Further, these studies show the utility of targeting the acid−base catalyst using appropriately positioned positively charged nitrogen atoms, as well as the challenges associated with aglycon substitutions.

Glycoside hydrolases (or glycosidases) are an important class of enzymes that have roles in processes ranging from biomass degradation to viral recognition. The rapid pace of genomic sequencing suggests that tens of thousands of genes coding for putative glycoside hydrolases will soon be identified. Based on sequence conservation these can be classified into specific families (*1*). Currently the database of carbohydrate active enzymes (CAZy: http://www.cazy.org) lists 112 separate families of glycoside hydrolases.

The α1,3-α1,6-mannosidases, including lysosomal α-mannosidase (LM, E.C.3.2.1.24) and Golgi α-mannosidase II (GMII,[1] E.C.3.2.1.114) are members of the Family 38 glycoside hydrolases. These enzymes cleave the bond between 2 mannose residues with net retention of configuration and use a mechanism involving formation of a covalent glycosyl-enzyme intermediate. Lysosomal α-mannosidases are involved in the degradation of complex sugars derived from glycoproteins within the low pH environment of the lysosome. Impairment of LM activity, either through genetic mutation or environmental toxicity, leads to the buildup of partially processed oligosaccharides in large vacuolar structures within cells and has severe neurological consequences (*2, 3*). In contrast, Golgi α-mannosidase II is involved in the creation of glycoproteins that have complex carbohydrates appended. GMII is the final glycoside hydrolase in the N-glycosylation pathway and is responsible for the formation of the "core" trimannose structure. GMII catalyzes the hydrolysis of both an α-1,6 and an α-1,3 linked mannose from GlcNAc-Man_5-$GlcNAc_2$ (N-linked to an asparagine residue) to form GlcNAc-Man_3-$GlcNAc_2$-Asn. Subsequently a series of glycosyl transferases add a variety of carbohydrates (including *N*-acetyl glucosamine, galactose and sialic acid) to this trimannose core to form the completed complex carbohydrate structure.

Complex carbohydrates are implicated in the process of metastasis (*4, 5*). Amelioration of the metastatic phenotype through inhibition of the machinery of complex carbohydrate formation would provide an important weapon in the arsenal of cancer treatment (*6, 7*). Indeed initial clinical tests indicated that the GMII inhibitor swainsonine (which inhibits

[†] D.R.R. holds funding from the Canadian Institutes for Health Research (MOP79312) and the Mizutani Foundation (080032). S.G.W. receives funding from the Natural Sciences and Engineering Research Council of Canada and the Canadian Institutes of Health Research.

[‡] Coordinates for protein complexes reported in this manuscript are deposited in the Protein Data Base with accession numbers 3D4Y, 3D4Z, 3D50, 3D51, and 3D52.

* To whom correspondence should be addressed. Tel: (416)-581-7537. Fax: 416-581-7562. E-mail: drose@uhnresearch.ca.

[§] Ontario Cancer Institute.

[||] University of British Columbia.

[#] University of Toronto.

[1] Abbreviations: GMII, Golgi α1,3-α1,6-mannosidase II (E.C.3.2.1.114); dGMII, *Drosophila melanogaster* GMII; LM, lysosomal α-mannosidase (E.C.3.2.1.24); *Bt*Man2a, *Bacterioides thetaiotaomicron* GH2 retaining *β*-mannosidase; n.d., not determined.

10.1021/bi8010785 CCC: $40.75
Published on Web 08/30/2008

in the nanomolar range) had promise as a cancer treatment (*8*). However, side effects, in particular the inhibition of LM by swainsonine, severely limit its usefulness, necessitating the search for more specific inhibitors.

A common method of finding novel enzyme inhibitors is to screen large, divergent compound libraries, either *in vitro* or *in silico*. Based on the results of these assays, and in concert with data from structurally related compounds within the libraries, an initial indication of structure−activity relationships can be obtained, thereby forming the basis of a synthetic program for the development of more efficacious inhibitors. *In vitro* screening requires a well-defined assay adaptable to high-throughput automated methods. *In silico* screening requires the availability of a well-defined structural model for the protein target, generally obtained by X-ray crystallography, NMR methods or, in the absence of these, homology modeling.

Searching for new inhibitors with either *in vitro* or *in silico* methods is feasible with Golgi α-mannosidase II. Facile enzyme assays exist which measure the release of colored *p*-nitrophenol, 2,5-dinitrophenol, or fluorescent methylumbelliferyl alcohol from their respective conjugated α-mannopyranosides. As well, X-ray crystallographic data approaching atomic resolution are available for *Drosophila* GMII (dGMII) (*9, 10*). We have previously undertaken screening of the Maybridge chemical library of 50,000 compounds looking for compounds that inhibit dGMII in the micromolar range. Only a single compound having slight inhibitory activity was detected, but was not visible within the active site as assessed by X-ray crystallography (D. Kuntz, R. Donovan, A. Schimmer, D. Rose, unpublished). Analysis of positive hits from an *in silico* screen of a 200,000 compound virtual library making use of the Gold molecular docking algorithm (*11*) carried out by a commercial source (Protana Inc., Toronto, ON) gave no compounds that showed any dGMII inhibitory activity (D. Kuntz, D. Rose unpublished). The lack of success of the *in silico* method can be attributed to the fact that, first, docking into the zinc-containing active site pocket of dGMII is very difficult to model, and, second, Gold is not well suited to use with this enzyme (*12*).

The search for novel mannosidase inhibitors is aided by the fact that development of glycosidase inhibitors is a field of intense study by synthetic organic chemists. Currently marketed drugs resulting from these efforts include Glyset (miglitol) and Volix (voglibiose) for the treatment of type II diabetes as well as the anti-influenza drugs Relenza (zanamivir) and Tamiflu (oseltamivir). These studies have produced a large number of compounds, which may not have the desired activity against the target protein but may have serendipitous activity against related enzymes with slightly different substrate specificity. We have accumulated a number of these potential glycoside hydrolase inhibitors (currently about 500) from our own laboratories as well as those of generous collaborators and are screening this "focused library" against a wide panel of glycoside hydrolases. Thus far this approach has led to the identification and structural analysis of novel inhibitors for an endoglycoceramidase (*13*). In this paper we report on the use of this focused library to search for new inhibitors of dGMII and *Drosophila* LM. Interestingly, four of the five inhibitors found were previously identified as β-glucosidase inhibitors. Using X-ray crystallography we have determined the structures of these compounds in complex with dGMII. A comparison is then made with previous structures containing the inhibitors bound to various glucosidases, and with dGMII bound with other inhibitors.

EXPERIMENTAL PROCEDURES

Mannosidase Preparation. The catalytic domain of *Drosophila melanogaster* Golgi mannosidase II (dGMII) was expressed in a secreted form from cultured *Drosophila* cells (Schneider S2 cells). Purification of dGMII from culture medium using Cibacron Blue F3GA-agarose (Sigma, St. Louis MO) and nickel NTA-agarose (Qiagen, Dorval QC) was as previously described (*14*). The *Drosophila* lysosomal mannosidase (dLM) used in this study is the CG6206 gene product that was expressed in a similar manner in S2 cells. Briefly, the full-size cDNA clone (GH02419) encoding the protein was obtained from the Berkeley *Drosophila* Genome Project. The coding sequence was incorporated behind an amino-terminal His_6-tag into a modified pMT/BiP/V5-His vector (InVitrogen, Carlsbad, CA), which carries the BiP signal for secretion. This vector results in secretion of expressed protein into the media of transfected S2 cells. Cells were transfected using calcium phosphate, selected using blasticidin (Calbiochem, San Diego, CA) and single cell clones expressing the highest levels of PNP-α-D-mannopyranoside (Sigma) degrading activity were selected. Large-scale expression was carried out in serum-free medium (EX-CELL 420, JRH Biociences, Lenexa, KS). During expression the amino-terminal His_6 tag was lost. Purification was carried out using an initial salt elution from Blue-Agarose followed by purification on an anion exchange resin (Q-Sepharose FF, GE Biosciences, Montreal, PQ).

Library Screening. 2,5-DNP-α-D-mannopyranoside was prepared as described previously (*15*). The kinetic analyses were run as continuous assays at room temperature using 2,5-DNP-α-D-mannopyranoside (2 mM) as the substrate with detection of the released dinitrophenolate anion by UV/vis spectroscopy at 400 nm. dLM was assayed in 50 mM sodium acetate buffer at pH 4.5 while dGMII was assayed in a buffer containing 50 mM MES, pH 5.6, 0.1% BSA and 0.1% $ZnSO_4$. Inhibitors were identified from a medium-throughput screen of a library of approximately 500 potential glycosidase inhibitors assembled in the Withers laboratory. This screen was performed on a Beckman Coulter BiomekFX liquid handler with an integrated plate reader operating in UV/vis absorbance mode (400 nm). The screen was performed in 384 well plates, with each well containing a final volume of 60 μL, and was based on a microformat of the conditions described above. Each compound was assayed at two concentrations (10 and 100 μM) and compounds showing statistically reduced activity were investigated further using full enzyme kinetic analysis on a Varian Cary 300 or Cary 4000 UV/vis spectrophotometer. Range-finder K_i values were determined using a fixed concentration of substrate, 2,5-dinitrophenyl α-D-mannoside (2 mM), and inhibitor concentrations ranging from 0.2 to 5 times the K_i value ultimately determined. A horizontal line drawn through $1/V_{max}$ in a Dixon plot of these data ($1/V$ vs [I]) intersects the experimental line at an inhibitor concentration equal to $-K_i$.

Table 1: Data Collection and Refinement Statistics for *Drosophila* Golgi Mannosidase II Complexes Reported in This Study

	1	2	3	4	5
ligand code	MVL	GIM	OEV	GOX	GHR
PDB code	3D4Y	3D4Z	3D50	3D51	3D52
			Data Collection		
X-ray source	CHESS A1	CHESS F1	rotating anode	CHESS A1	CHESS A1
cell dimensions (Å)	68.6 × 108.9 × 137.0	68.6 × 109.3 × 137.8	68.8 × 110.0 × 138.1	68.7 × 109.1 × 137.7	68.6 × 107.9 × 137.1
resolution (Å)					
overall	30−1.52	30−1.39	20−1.79	40−1.43	20−1.60
high resolution shell	1.54−1.52	1.41−1.39	1.83−1.79	1.46−1.43	1.63−1.60
% completeness (overall/hi_res)	99.2/96.4	99.5/97.5	98.5/83.7	98.8/83.5	97.4/96.9
unique reflections (obsd/theor)	156781/ 158024	207007/ 208122	97944/ 99421	188859/ 191100	131084/ 134545
redundancy (overall/hi_res)	6.05/4.3	7.03/5.15	4.2/2.0	6.8/1.6	4.99/5.3
I/σ (overall/hi_res)	11.2/2.6	19.4/5.9	14.5/2.6	15.5/2.9	13.7/7.27
R_{merge} (overall/hi_res)	0.084/0.514	0.061/0.235	0.061/0.378	0.077/0.250	0.087/0.208
			Refinement		
program (final refinement)	Refmac	Shelx	Refmac	Refmac	Refmac
R/R_{free} for all reflns	0.186/0.208	0.144/0.181	0.156/0.187	0.187/0.201	0.228/0.240
R/R_{free} for $Fo > 4\sigma$		0.135/0.170			
atoms in model	9444	9416	9508	9408	9128
amino acids	1016	1016	1016	1016	1016
alternate conformers	11	9	14	12	2
water molecules	1104	1135	1174	1127	875
rmsd bonds (Å)	0.018	0.011	0.023	0.013	0.017
rmsd angles (deg)	1.77	2.0	1.91	1.53	1.86
average B factors (Å^2)					
overall	26.4	17.9	16.0	16.9	17.1
protein main chain	22.6	14.1	13.4	13.9	14.5
protein side chain	24.4	18.3	15.5	16.4	17.4
water	40.9	30.0	26.7	29.1	27.9
bound compound	23.9	9.4	17.4	13.2	24.7
others (MPD, NAG, Zn)	26.4	19.5	43.6	19.4	19.2

Crystallization. Crystals of unliganded dGMII were grown using the hanging-drop vapor diffusion method in Tris-buffered precipitation solution (*14*) using dGMII crystal seeds as the nucleation agent. Seeds were prepared using the Seed Bead Kit (Hampton Research, Aliso Viejo, CA). Due to the presence of Tris, which may interfere with the binding in the active site, crystals were washed in MOPS buffered reservoir solution (MBRS) (0.1 M MOPS pH 7.0, 8.5% (w/v) PEG 6K 2.5% (v/v) MPD) followed by a 16−24 h soak in MBRS containing 2 mM inhibitor. Crystals were then passed through solutions of MBRS with 1 mM inhibitor and increasing concentrations of MPD (10, 15, 20, 25% v/v) for cryoprotection. Crystals were flash frozen in liquid nitrogen.

Data Collection. X-ray diffraction data were collected at 100 K on a Bruker home source or at the Cornell High Energy Synchrotron Source beamlines A1 and F1. Data were integrated HKL2000 (*16*), or SAINT (Bruker AXS Inc., Madison, WI). Scaling was carried out using SADABS (Bruker). A constant set of R_{free} data was created by reading the data into CCP4 (*17*) and merging with a previous R_{free} data set. The data was then written in mtz, cns, and hklf4 formats for use in subsequent refinement programs.

Refinement of dGMII Inhibitor Complexes. The structures of the complexes were initially phased by molecular replacement using the software program CNS (*18*). Rigid body refinement was carried out against the published structure of native dGMII (PDB 1HTY) with Tris and waters in the region of the active site removed. This was followed by simulated annealing to 3500 K, group B-factor refinement, and individual B-factor refinement. At this stage the $F_o - F_c$ density clearly indicated the presence or absence of bound compound. Additional water molecules were picked using the Arp/Warp routine (*19*) in CCP4. Ligand molecule dictionaries and starting coordinate files were generated using the ProDrg server (http://davapc1.bioch.dundee.ac.uk/programs/prodrg/). Ligand fitting and verifying proper fit to the electron density was performed using the program Coot 0.31 (*20*). REFMAC5 (*21*) refinement was then iterated with Coot fitting. For high resolution refinement of the dGMII:GIM complex SHELX97 (*22*) was used. CGLS refinement to increasing resolution was followed by refinement of anisotropic B-factors. Statistics for data collection and refinement are presented in Table 1. The quality of the final models was assessed using a number of structure validation programs including MolProbity (http://molprobity.biochem.duke.edu/) and the RCSB Validation Server (http://deposit.pdb.org/validate/). Protein overlays for the comparison of inhibitor binding were carried out using the SSM Superpose subroutine of Coot (*23*). During the overlay with 1PS3 it was noted that the kifunensine in the active site had unusual bond lengths. Real space refinement of the kifunensine and associated waters in the active site region was carried out with Coot using structure factors available from the Protein Data Bank (PDB) (*24*). Graphics were generated using PyMOL (http://pymol.sourceforge.net).

RESULTS AND DISCUSSION

Both *Drosophila*-derived Golgi α-mannosidase II and lysosomal mannosidase were screened against a focused library of about 500 compounds that had been assembled through previous studies of carbohydrate-specific enzymes. On the basis of this screen, five previously unidentified inhibitors of these mannosidases were found, some of which bind in the low micromolar range (Figure 1). This success rate contrasts vividly with previous experience with nonfo-

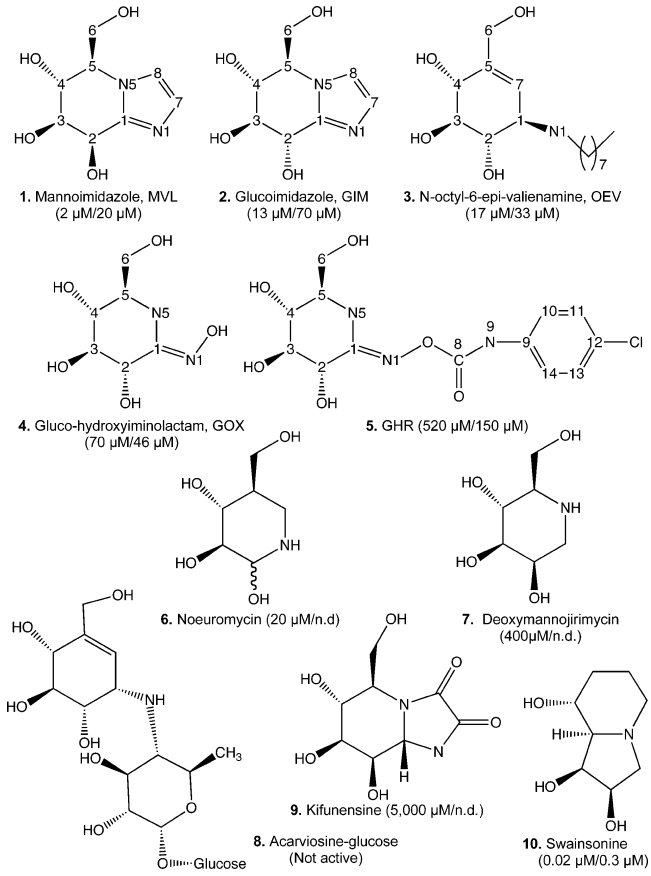

FIGURE 1: Compounds discussed in this paper. The structures of compounds **1**−**5** in complex with *Drosophila* Golgi α-mannosidase II (dGMII) are determined in this paper. For these compounds the common name and the three-letter code used in the PDB submission are indicated. Values in parentheses represent the measured K_i for dGMII and *Drosophila* lysosomal α-mannosidase respectively; n.d. is not determined. Atoms are numbered to most closely represent the numbering of the carbohydrate on which they are based.

cused libraries, especially given the fact that the majority of these compounds were synthesized as inhibitors of glucosidases and not mannosidases. The best of these represent very reasonable leads for drug development. Further investigation, therefore, was undertaken in order to understand how gluco-configured inhibitors could bind so well to a mannosidase.

The tightest binding inhibitor, mannoimidazole (MVL, compound **1**), has a K_i of 2 μM for dGMII and is about 10-fold more potent on the Golgi enzyme than it is on the lysosomal homologue. The next most proficient inhibitor was glucoimidazole (GIM, compound **2**), which differs from MVL in the stereochemistry of the oxygen at C2. (For the purposes of this paper these compounds have been numbered to most closely reflect the numbering of the sugars that they mimic rather than by strict IUPAC rules. The numbering, and the three letter abbreviations, for the compounds shown in Figure 1, are the same as those of the compounds in structures deposited in the PDB). Despite the fact that GIM is a glucose analogue, its K_i is only about 7-fold lower than that of MVL. Glucoimidazole also shows selectivity for the Golgi enzyme over the lysosomal enzyme. Another hit with a comparable inhibition profile is *N*-octyl 6-*epi*-valienamine (OEV, compound **3**), which is slightly less selective than GIM or MVL for the Golgi homologue. This compound is not only "gluco" configured at C-2, but also has an equatorial C-1 substituent, equivalent to a β-glucoside. Gluco-hydroxyiminolactam (GOX, compound **4**) is about 5-fold less inhibitory than the other two gluco-homologues and is more selective for the lysosomal enzyme, while the addition of a long aromatic tail to GOX, to give GHR (compound **5**), results in a further loss of both GMII inhibition and selectivity.

X-ray crystallographic analyses were carried out on complexes of each of these newly discovered inhibitors to investigate their mode of binding to dGMII. To this end, crystals of dGMII were first grown in Tris-buffered crystallization solution. Previously we have noted that the high concentrations of Tris in the crystallization solution competed with the binding of lower affinity inhibitors to the active site (*25*). In the experiments reported here the dGMII crystals were first washed with a Tris-free MOPS buffered crystallization solution, prior to soaking the crystals overnight with the inhibitors in this solution. Crystals were then frozen in liquid nitrogen prior to data collection. High resolution, redundant data sets were collected for each complex and these were subjected to crystallographic refinement. The statistics for data collection and refinement are given in Table 1. Overall, the final refinement statistics for this group of crystal structures are slightly worse than those of previously determined dGMII structures. There is a slight overall shrinkage in the unit cell (normally close to 69 Å × 110 Å × 139 Å), which may be a result of the soaking medium used for this set of crystals. Despite this caveat, the electron density for the bound compounds was clear in the initial omit maps and unambiguous modeling of the inhibitors (except for the long side chain of GHR, see below) was possible.

An example of the electron density seen in the active site region is shown in Figure 2, which illustrates the $2F_o - F_c$ density for the dGMII:GIM complex. This figure demonstrates how well defined the electron density is for both the protein and the inhibitor in this 1.4 Å structure. This figure, which is a view into the active site pocket, also shows how tightly associated the inhibitor is with the active site. Simulated annealing $F_o - F_c$ omit maps are shown for MVL, GIM, OEV, GOX, all in identical orientation (Figure 3). For GHR, the final $2F_o - F_c$ map is provided, showing the density in each of the putative locations for the poorly resolved aglycon portion. Two likely conformations of the aglycon are modeled. In all cases the density for that portion of the compound in close apposition to the zinc is very clear, and the ring conformation can be easily determined.

A comparison of bound mannoimidazole and glucoimidazole is shown in Figure 4A. Overall the two compounds occupy a very similar position in space, with the imidazole being slightly skewed. The O2 and O3 hydroxyls make tight contacts with the active site zinc, and end up very closely juxtaposed in space despite the difference in stereochemistry at the C2 position. The O4 and O6 also end up in very similar positions, making contacts with Asp472 and the main chain carbonyl of Arg876 respectively. Close interactions (less than 3.2 Å) of the compounds with elements of the dGMII structure are detailed in Figure 5. Figure 5A details the dGMII:MVL complex interactions while Figure 5B outlines the comparable dGMII:GIM distances. It is clear that there is very little difference in the interactions made by GIM or MVL to dGMII, with the most significant being the interactions made at O2. In the dGMII:MVL structure the O2 is 2.1 Å from the active site zinc and 2.5 Å from Oδ2 of the

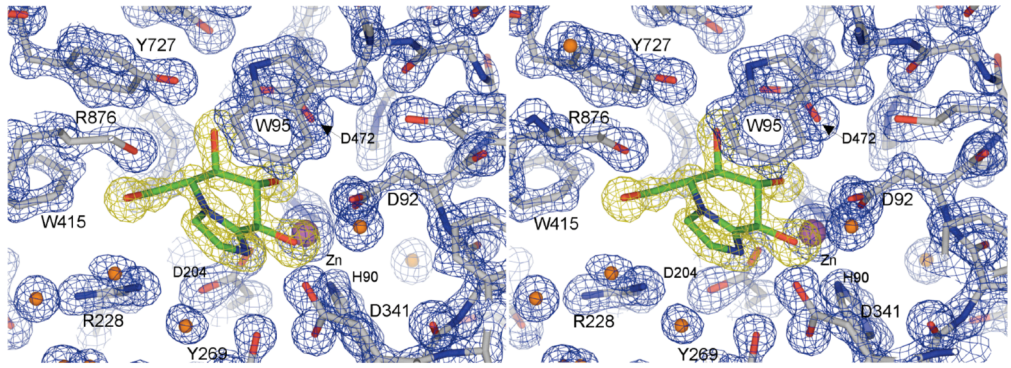

FIGURE 2: Stereoview of the electron density observed in the active site of the dGMII:GIM complex. The $2F_o - F_c$ electron density map (blue) is contoured at 2σ while the simulated annealing omit $F_o - F_c$ map (yellow) is contoured at 4σ. Carbons of the amino acid side chains are colored gray, and of GIM are colored green. Waters are represented as orange spheres, and the active site zinc residue is represented as a magenta sphere. Residues making important contacts are labeled. These include W95 which forms the lid of the active site pocket and makes a stacking interaction with the carbohydrate ring. H90, D92, D204 (catalytic nucleophile), D341 (acid/base catalyst), D472, Y727 and R876 make direct hydrogen bonds, and R228 makes a through water hydrogen bond. W415 makes hydrophobic interactions, while Y269 closely interacts with other active site residues and forms H-bonds in other complexes.

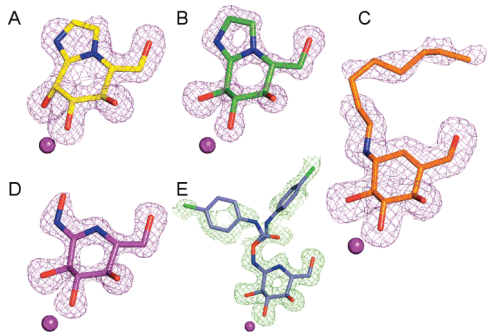

FIGURE 3: Electron density observed bound in the active site of the dGMII complexes studied and the fitted models of the inhibitor. The magenta electron density A−D represents $F_o - F_c$ simulated annealing omit maps. The green electron density in E is the final $2F_o - F_c$ map and shows the positions of 2 possible conformations of the aromatic side chain. A: MVL, contoured at 3σ. B. GIM contoured at 5σ. C. OEV contoured at 2.8σ. D. GOX contoured at 4σ. E. GHR contoured at 0.9σ.

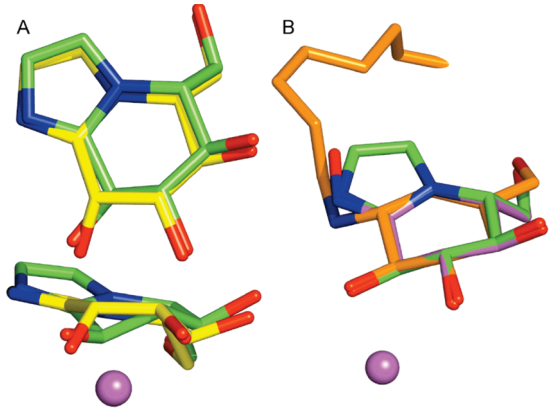

FIGURE 4: Comparison of conformations of the inhibitors bound in the active site of dGMII. A. Comparison of mannomidazole (MVL, yellow) and glucoimidazole (GIM, green) B. Comparison of the gluco-form inhibitors GIM (green), OEV (orange) and GOX (magenta). Complete structures were superimposed using the SSM algorithm in Coot and the coordinates for the inhibitor extracted for comparison. The magenta sphere represents the active site zinc complex whose position was extracted from the dGMII:GIM complex and is included as an aid to orientation.

catalytic nucleophile residue Asp204. In this case the Asp204 Oδ2 is 2.2 Å away from the zinc. In the dGMII:GIM structure the O2 is further away from the zinc (by 0.34 Å) while the Asp204 Oδ2 moves closer (now 2.1 Å). The Asp 204 Oδ2 is also 0.5 Å further away from O2 in the GIM structure compared to what is seen in the MVL complex.

The acid−base catalyst residue Asp341 interacts with the N1 position of the imidazole ring, which occupies a position comparable to the oxygen of the scissile glycosidic linkage in the natural substrate. This is in accord with the expected mode of action of these inhibitors; the imidazoles and hydroxyiminolactams possess a heteroatom in the ring plane that was incorporated to promote strong hydrogen bonds with acid/base residues, and mimic the lateral protonation that occurs during catalysis (*26*). Given the fact that there is only a reasonably small difference (7-fold) in inhibition constants between the gluco and manno-configured imidazoles, the interaction with N1 must yield disproportionately more to binding than do the two carbohydrate fragments, and is probably largely responsible for the strong inhibition seen. Further discussion about the role of the acid−base catalyst residue in promoting inhibitor binding is provided below.

An overlay of three glucose-like inhibitors (GIM, OEV, and GOX) extracted from their respective complexes is shown in Figure 4B. It is clear from the overlay that all three gluco headgroups are bound in a nearly identical manner in the active site of dGMII. The only significant difference is the C6 of OEV, which is flattened because of the double bond at this position. However the O6 of OEV, which makes contacts with the Arg867 carbonyl, is in a similar position to that seen in the other compounds. Interaction distances for OEV, GOX, and GHR are shown in Figures 5C to E respectively. All the distances are very comparable between the four glucose-like inhibitors.

A large part of the synthetic effort in the design of glycosidase inhibitors is devoted to the creation of transition-state mimics, with carbohydrate rings distorted from the low energy $^4C_1$ conformation normally found in solution into a conformation more resembling what is expected in the enzyme at the transition state. By restricting the inhibitors to a reduced conformational itinerary, the energy expenditure normally required for distortion of the substrate toward its transition-state conformation (on the order of 10 kcal/mol for carbohydrates) will be eliminated and the inhibitors will bind more tightly than the natural substrate. Structural and

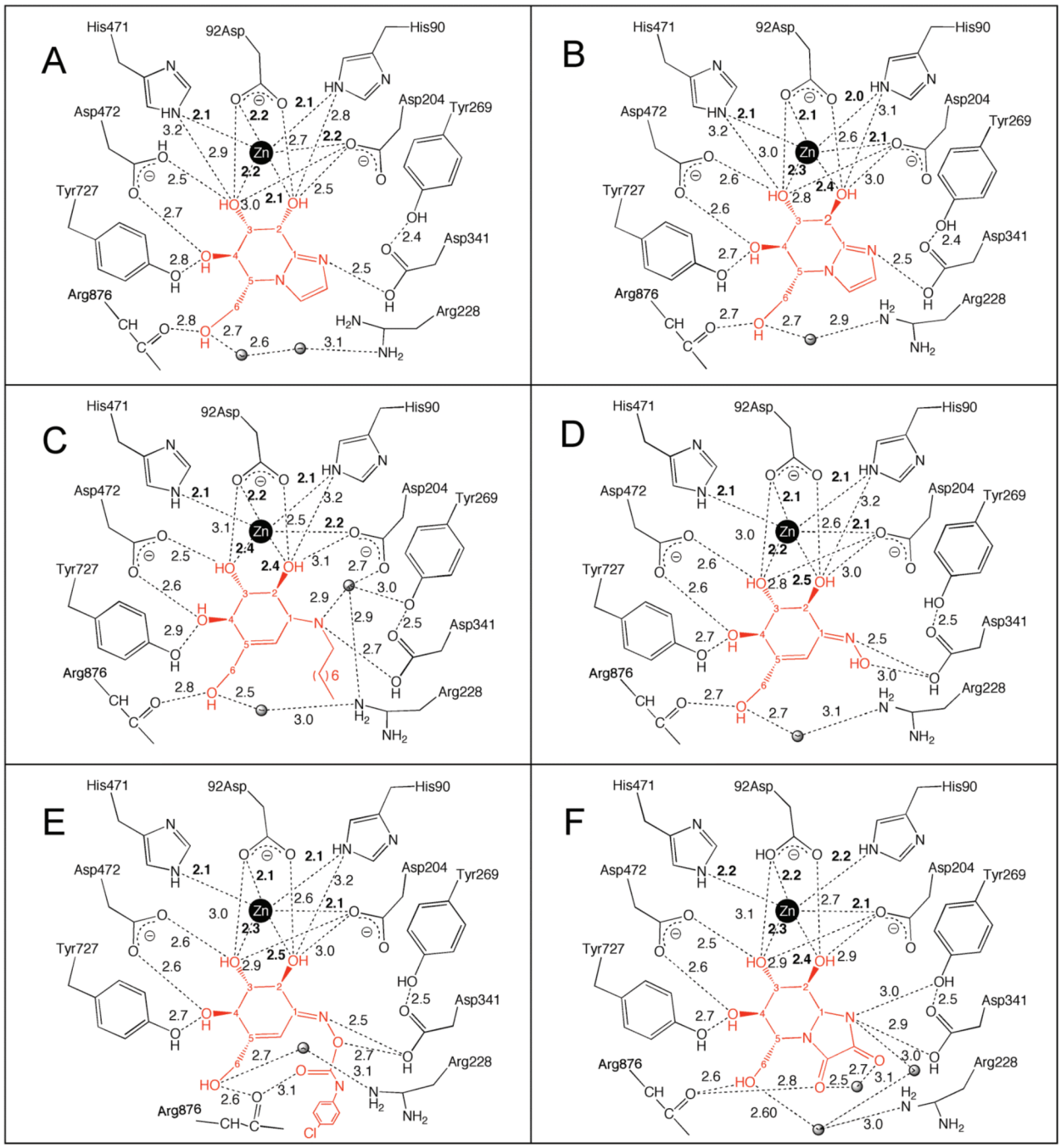

FIGURE 5: Close interactions between the bound inhibitors and active site residues of dGMII observed in the X-ray crystallographic structures. Distances less than 3.2 Å are indicated. Bound inhibitors, numbered as in Figure 1, are colored red, and water molecules are represented as gray spheres. The panels are (A) MVL, (B) GIM, (C) OEV, (D) GOX, (E) GHR and (F) kifunensine.

kinetic evidence suggests that the conformational itinerary is enzyme-dependent varying even among related glycosidases (*27*), thus necessitating the design of a range of conformational mimics. Despite the difficulties, this approach has led to some spectacular successes, one of the most noteworthy being GlcNAcstatin, a 5 pM inhibitor of O-GlcNacAse, which X-ray crystallography revealed to be a transition-state mimic (*28*). This approach has also been very successful with the glucoimidazoles (*29, 30*), which are nanomolar inhibitors of some β-glucosidases. Mannoimidazole was reported to be a potent inhibitor of snail β-mannosidase ($K_i = 55$ nM), and galactoimidazole was very active against an *Escherichia coli* β-galactosidase ($K_i = 4$ nM) (*29*). The reported results of an X-ray analysis of the glucoimidazole hydrochloride salt showed a $^5H_6$ conformation ($^5H_4$ based on sugar notation) in the solid state and a $^6H_7$ ($^4H_3$) conformation in D_2O while the mannoimidazole adopted what was termed an E_7 (E_3) conformation (*29*). The MVL in the dGMII complex is in what can best be described as a $^4H_3$ conformation, similar to that reported for GIM in solution. This is different from the expected $B_{2,5}$ transition-state conformation for dGMII (*31*), and thus MVL is not acting as a transition-state mimic for this enzyme.

The structures of a number of inhibitors, including mannoimidazole, bound to a bacterial GH2 retaining β-mannosidase (*Bt*Man2a) have recently been reported (*32*). In the complex with MVL (PDB 2VMF) (which had a K_i of 1.4 μM, similar to what was seen with dGMII), the inhibitor

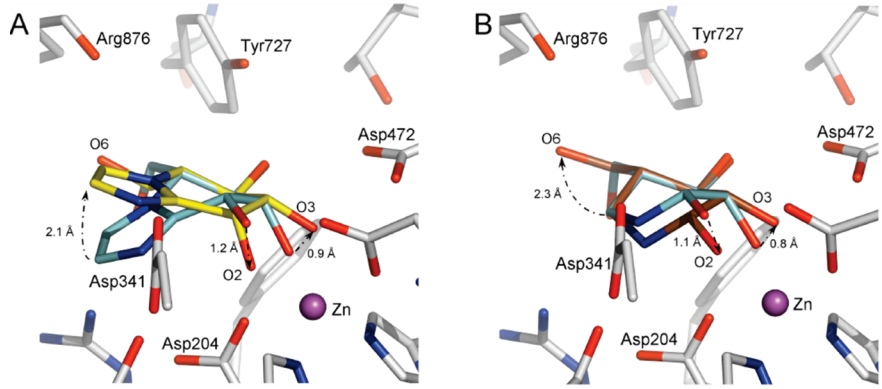

FIGURE 6: Mannoimidazole and noeuromycin bound in the active site of dGMII are distorted differently than when bound to the β-mannosidase *Bt*Man2a. A. Comparison of mannoimidazole binding. dGMII bound inhibitor is colored yellow, and *Bt*Man2a (from PDB 2VMF) is colored cyan. B. Comparison of noeuromycin binding. dGMII bound inhibitor (from PDB 2ALW) is colored brown, and BtMan2a (from PDB 2VL4) is colored cyan. dGMII amino acid side chains are shown in gray, and the active-site zinc is colored magenta. For clarity Trp95 is not shown. The coordinates for the inhibitors were extracted from the non-dGMII PDB files, and manually superposed with the dGMII structure using the coordinates of C3, C4 and C5 as the basis for the superposition.

was found distorted into a $B_{2,5}$ conformation, which is the expected conformation for the transition state. In this case, addition of aryl substituents, which bind in the tryptophan-rich aglycon site, lead to an approximate 20-fold reduction in K_i values. A comparison of MVL bound to dGMII or *Bt*Man2a is shown in Figure 6A, where the difference in conformation is clear. The zinc had pulled the O2 by over 1 Å, while the O3 has moved up toward the Asp472. The imidazole ring has moved significantly (2.1 Å at the C8 position) and now makes a close interaction with the acid−base catalyst Asp341, while the O6 has swung to make interactions with Arg876 carbonyl group.

In the same paper Tailford et al. examine the interaction of *Bt*Man2a with noeuromycin (*32*). Noeuromycin is an isofagomine-like compound which differs from deoxynojirimycin in that the nitrogen, which mimics the positive charge in the oxocarbenium ion reaction intermediate, is positioned at the C1 position (anomeric carbon) rather than at the ring oxygen position (*33*) (see Figure 1). Isofagomine, was shown to inhibit more potently β-glucosidases in comparison to α-glucosidases (*34*), indicating that the position of the charged group is differentially recognized in the two groups of enzymes.

Noeuromycin exists as a mixture of two forms, a gluco-form, which is analogous to deoxynojirimycin, and a manno-form, which is analogous to deoxymannojirimycin (DMNJ). DMNJ is a potent inhibitor of the α-1,2 mannosidases (*35*), but we have previously shown it to be a weak (IC_{50} = 400 μM) inhibitor of dGMII (*14*). In contrast noeuromycin inhibited dGMII in the micromolar range. The crystal structure of the dGMII:noeuromycin complex showed that the enzyme extracted the manno-form, which was bound in what was best described as a $^{1,4}B$, although it had some $^{1}S_5$ character (*36*). The results of Tailford *et al.* show that, similarly to dGMII, the β-mannosidase BtMan2A was more strongly inhibited by noeuromycin than by DMNJ. The crystal structure revealed that the manno-form was extracted by *Bt*Man2A and was bound in a distorted conformation that was described as being close to $^{1}S_5$ and $B_{2,5}$. An overlay of the noeuromycin extracted from the dGMII structure (PDB 2ALW) manually superimposed with that from the *Bt*Man2A structure (PDB 2VL4) indicates that the two structures differ from each other, particularly at the crucial O2 and O3

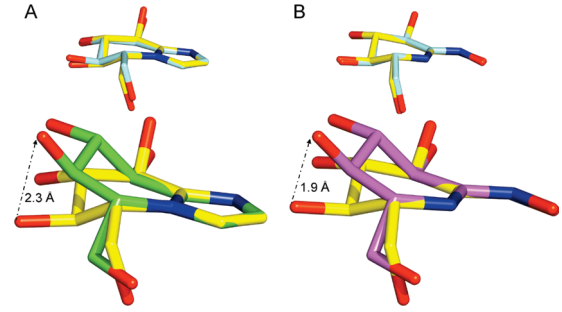

FIGURE 7: GIM and GOX bound in the active site of dGMII are distorted in comparison to previously published structures. A. Comparison of GIM bound to the active site of Family 1 β-glycosidase from *T. maritima* (yellow, from PDB 2CES) with that bound in *S. sulfataricus* β-glycosidase (cyan, from PDB 2CEQ) or dGMII (green). B. Comparison of GOX bound to the active site of β-glycosidase from *T. maritima* (yellow, from PDB 2J78) with the thio-β-glycosidase, myrosinase, from *Brassica* (cyan, from PDB 1E6S) or dGMII (magenta). The coordinates of the nitrogens and intermediate carbon atoms were used as the basis for the manual superposition.

residues (Figure 6B). The O2 is moved 1.1 Å toward the zinc, drawing the ring nitrogen down 0.7 Å toward the catalytic nucleophile Asp204, while the O3 moves upward 0.8 Å toward Asp472. At the same time the O6 swings 2.3 Å to make its interaction with the backbone carbonyl of Arg876.

A number of the compounds identified in the present study have been previously observed bound in the active sites of other glycoside hydrolases. GIM has been reported in complex with the Family 1 β-glycosidases from *Sulfolobus sulfataricus* (PDB 2CEQ) and *Thermotoga maritima* (PDB 2CES) (*37*). These enzymes can hydrolyze both β-glucosides and β-galactosides equally well and are inhibited by GIM with K_i values of 53 nM and 138 nM respectively (*37*). Figure 7A shows a comparison of the structure of GIM bound to the β-glycosidases manually superposed with that found in the active site of dGMII. While nearly identical conformations of GIM are seen within the Family 1 structures (inset), the carbohydrate ring is obviously distorted in the dGMII complex. The conformation of GIM is $^{2}H_3$ in the dGMII complex, differing from the ^{4}E conformation reported in β-glycosidase structures (*37*) or the E_3 or $^{4}H_3$ conformation of the unbound compound.

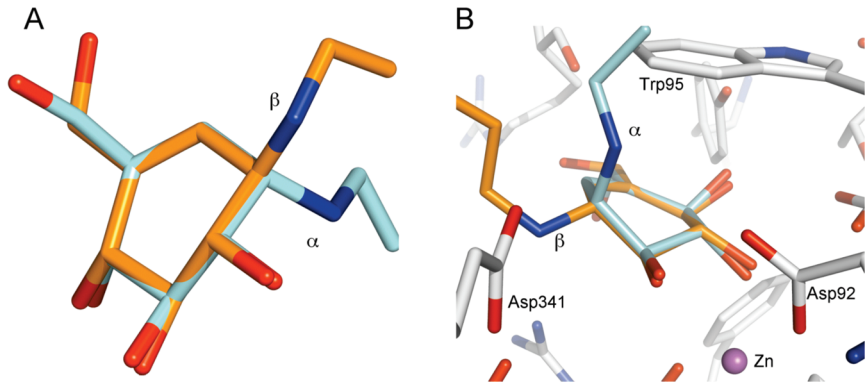

FIGURE 8: The valienamine moiety of OEV binds with an identical conformation to that found in acarbose. A. Comparison of dGMII bound OEV (orange) with the valienamine portion of acarbose analogue **7** bound to human α-amylase (cyan, from PDB 1XCW). B. Binding of an α-configured OEV would lead to spatial clashes. OEV bound in the active site (orange) in comparison with a superposed α-form. The coordinates of the ring carbons were used as the basis for the manual superposition.

Valienamine is an essential core unit of many α-glucosidase inhibitors, including acarbose. Acarbose (Precose) is pharmaceutically important in the treatment of type-II diabetes, acting through inhibition of both α-amylases and *exo* α-glucosidases. Valienamine is thought to mimic both the charge and ring distortion of the transition state. The conformation of the inhibitor is imposed by the double bond between C1 and C5. The $^{2}H_{3}$ conformation resembles some aspects of both the $^{4}H_{3}$ and $^{2,5}B$ conformations that are predicted to be the transition-state conformations for α-glucosidases. *N*-Octyl-6-*epi*-valienamine (OEV), which is "*β*-configured", has been found to be a potent *β*-D-glucocerebrosidase inhibitor (IC_{50} of 30 nM vs 17 μM for an α-glucosidase (*38*)) and may be useful in the treatment of Gaucher disease by serving as a pharmacological chaperone (*39, 40*). Unfortunately, there is no complex in the PDB with OEV bound. There are, however, a number of structures available in the PDB containing bound acarbose analogues, which have valienamine as a component. In Figure 8A we have compared the structure of OEV bound to dGMII with the valieneamine component in PDB 1XCW. PDB 1XCW consists of the structure of a trisaccharide based on acarbose (acarviosine-glucose, **8**) bound to human α-amylase (K_i = 75 nM (*41*)). It is clear from this structural comparison that the conformation of the carbohydrate-mimicking region is almost identical in the two complexes and best described as $^{2}H_{3}$, the favored solution phase conformation. In the half-chair extracted from PDB 1XCW the C1, C3, C4, and C5 atoms make a perfect plane while in the dGMII structure C3 is slightly below the plane. Thus while the O2's of the overlapped structure are 0.05 Å apart, the O3's and O4's differ by 0.43 Å and 0.3 Å respectively. This is the only example of a substance bound to native dGMII which is not distorted in some way from its expected low-energy solution phase conformation. It is not that the valienamine ring cannot be distorted, since the structure of 6-*epi*-valienamine bearing an acetamido group (a GlcNAc analogue) bound to a Family 84 *β*-hexosaminidase from *Bacteriodes thetaiotaomicron* shows the unsaturated ring to be quite distorted (*42*). The major difference in the two inhibitors, as shown in Figure 7A, is in the "α" (*S*) or "*β*" (*R*) nature of the attached substituents. Manually docking the α-configured valienamine into the active site of dGMII leads to clashes between atoms attached to the α-configured nitrogen and Trp95, which forms the lid of the catalytic site (Figure 8B). Thus, valieneamine-based inhibitors bearing α-configured substituents would not be expected to be effective against GMII, indeed none of these compounds (which were present in the focused screen) showed any activity against dGMII.

The original publication of the synthesis of D-glucohydroxyimino-1,5-lactam (GOX, **4**) and its *N*-arylcarbamate derivative (GHR, **5**) reported K_i values of 0.6 μM and 0.8 μM, respectively, against the *β*-glucosidase from *Agrobacterium sp.* and 16 μM and 21 μM, respectively, against the *β*-glucosidase from almonds (*43*). A derivative related to GHR with a chlorine atom at the position 1 instead of 3 in the aryl ring was more potent than GOX (K_i of 0.15 μM and 8 μM against the two aforementioned enzymes (*43*)). Structural analysis by small molecule X-ray crystallography and NMR spectroscopy in D_2O indicated that GOX adopts a conformation between $^{4}C_{1}$ and $^{4}H_{3}$ in the solid state and $^{4}C_{1}$ in solution (*43*).

GOX has previously been shown bound to two different Family 1 glycoside hydrolases, the strongly inhibited *β*-glycosidase from *T. maritima* (PDB 2J78) (K_i = 0.28 μM (*44*)) and the unusual thio *β*-glycosidase, myrosinase, from *Brassica* (PDB 1E6S) which is only weakly inhibited (K_i = 600 μM (*45*)). The conformation of the bound compound in these Family 1 structures is nearly identical, as seen in Figure 7B (inset). In contrast, GOX bound to dGMII is considerably different. The conformation of GOX bound to the family 1 enzymes is $^{4}H_{3}$ and to dGMII is $^{2}H_{3}$. Consequently while C1, C2, N5 and N1 are separated by less than 0.1 Å, in the overlapped structures O2, O3 and O4 are separated by 0.6 Å, 1.2 Å, and 1.9 Å respectively (Figure 7B).

We next compared the binding of our newly discovered inhibitors with previously solved X-ray structures of dGMII inhibitor complexes. A very high degree of similarity was found with the previously determined structure of dGMII bound to kifunensine (PDB 1PS3, K_i = 5 mM (*25*), Figure 9A). On the other hand, swainsonine, the most potent inhibitor of GMII (with a K_i of about 40 nM), binds to dGMII in a manner that was quite different from MVL (Figure 9B). MVL also binds in a position that is quite different from that seen for either bound mannose (Figure 9C), which is in a high energy $B_{2,5}$ boat conformation (PDB 3BUP (*10*)) or the trapped covalent intermediate, which is in a $^{1}S_{5}$ skew boat (Figure 9D) (PDB 1QWN (*31*)), although the positions of its tightly bound hydroxyl groups (at the 2, 3 and 4 positions) are quite similar. The conformations found for the

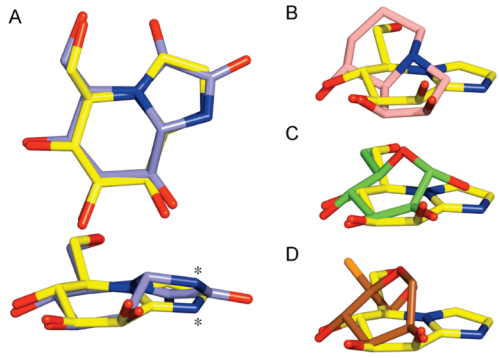

FIGURE 9: Mannoimidazole binding to dGMII is similar to that of kifunensine. A. Two views comparing the position of bound MVL (yellow) with bound kifunensine (slate, from PDB 1PS3). The asterisks indicate the positions of the nitrogens that interact with the acid−base catalyst Asp341. B. Comparison of MVL binding with that of the nanomolar inhibitor swainsonine (salmon, from PDB 3BLB). C. Comparison of MVL binding with bound mannose (green, from PDB 3BUP). D. Comparison with the covalently trapped mechanism-based inactivator, 5-fluoro-β-L-gulosyl fluoride (brown, from PDB 1QWN). Complete structures were superimposed using the SSM algorithm in Coot and the coordinates for the inhibitor extracted for comparison. The hydroxyls that bind zinc point toward the reader.

bound inhibitors studied here are $^{2}H_{3}$ or $^{4}H_{3}$, and are not expected to be on the conformational itinerary of dGMII cleavage, and are thus clearly not transition-state mimics. An explanation for the inhibitory competence came from a comparison with the poor dGMII inhibitor kifunensine.

Kifunensine is a very strong inhibitor of class I endoplasmic reticulum α1,2-mannosidase (ERMI, a Family 47 Ca^{2+} dependent inverting enzyme) with a K_i of 100 nM against the enzyme from rat (*46*) while it is only a millimolar inhibitor of dGMII. Kifunensine binds in a low energy $^{1}C_{4}$ conformation to human ERMI (*47*) but in a distorted $^{1,4}B$ conformation to dGMII (*24*). The inhibitor positions extracted from a superposition of the dGMII:kifunensine (PDB 1PS3) and the dGMII:MVL structures are shown in Figure 9A and are very close, with the exception of the difference in the conformation of the sugar ring. MVL, however, demonstrates a 2500-fold lower K_i than what was reported by Shah (*24*) for kifunensine. The interactions made with the active site of dGMII are detailed in Figure 5E (these values are for a corrected version of PDB 1PS3, see Experimental Procedures). There are actually more close interactions in the kifunensine complex, including 2 waters that are closely apposed to the vicinal carbonyl groups, than are seen in the dGMII:MVL structure, so it is not clear what contributes to the much increased potency of the imidazole. There is certainly a "conformational cost" required for the distortion of the kifunensine into the higher energy boat conformation that is required for the interaction with the zinc (*24*). This conformational penalty would be less for the imidazole as the compound is already in a flattened conformation. A second major factor is that kifunensine has no charge since both of the nitrogens are amides, while the imidazole will be protonated and therefore will benefit from electrostatic interactions with the Asp341 acid−base residue in the active site. Indeed, the nitrogen and interacting Oδ2 are 0.4 Å closer in the dGMII:MVL complex than in the complex with kifunensine. Thus, it is probable that it is the presence of these fixed positive charges in the imidazole and hydroxyiminolactam-based inhibitors interacting with Asp341, rather than conformational transition-state mimicry, that is most important for the inhibitory effect of those compounds. As mentioned previously these compounds contain a ring plane heteroatom incorporated to mimic the lateral protonation that occurs during catalysis and promote strong hydrogen bonds with the acid/base catalyst. In the case of GMII this seems to be a very effective binding mode; compounds that are being distorted away from their low-energy conformation into a conformation that is not part of the enzyme's conformational itinerary, and thus clearly not transition-state mimics, can act as micromolar inhibitors, as shown here. This is highly analogous to the conclusions drawn concerning the binding modes of related inhibitors to a xylanase published recently (*48*) where kinetic experiments indicated factors other than transition-state mimicry are involved in some tight binding inhibitors. This is a currently unexploited avenue of study in the design of GMII inhibitors since very few of the known inhibitors make use of this mode of interaction.

For many glycoside hydrolases the addition of a +1 site binding aglycon mimic to an inhibitor that otherwise binds in the −1 site results in a product with increased affinity (e.g. refs *28, 29, 37, 43, 44, 49*−*51*). For GMII this has not been the case (e.g. refs *52, 53*) and the synthesis of chain-extended analogues generally results in an inhibitor of reduced potency. This is demonstrated in the current study with GHR, the extended analogue of GOX, of which the K_i dropped more than 7-fold on chain extension (Figure 1). Recent work investigating the binding of mannosidase substrate analogues and native substrate to a catalytic nucleophile mutant of dGMII (*10, 54*) indicates that there is actually very little binding in the +1 site, in contrast to what is found with other exoglycosidases. This is a consequence of the mechanism of GMII, which involves the cleavage of two mannose residues from $GlcNAcMan_5$ substrate in a single active site. The +1 residue serves as a swivel point, and the mannoses attached at the 6 and 3 positions are sequentially cleaved off. The required flexibility demands that the +1 swivel sugar not be tightly bound to the protein and is in fact found in multiple positions in complexes with substrate analogues (*10*). It is perhaps not surprising then that the GHR tail, intended to bind at a +1 site, is not found tightly bound to a single position but in at least 2 potential conformers. There is obviously some deleterious effect or interaction present as evidenced by the 7-fold reduction of inhibitory activity.

In conclusion, these studies of focused glycosidase inhibitor libraries have led to the identification of several new GMII inhibitors that bind in the micromolar range, whereas previous screens of random libraries were unsuccessful. Four out of five of the identified hits for this α-mannosidase were previously identified as β-glucosidase inhibitors. These studies highlight the ability of the GMII active site to deform compounds into binding entities that retain substantial inhibitory activity, even though they do not appear to be on the expected normal conformational itinerary of the enzyme and are thus not transition-state mimics. Further, they illustrate the utility of targeting the acid−base catalyst using appropriately positioned, positively charged nitrogen atoms, as well as the uncertainty of aglycon substitutions. Together these results will help guide future synthetic work toward potent, selective inhibitors.

ACKNOWLEDGMENT

We thank Tara Signorelli and Navleen Ghuman for help in cloning and purification of the lysosomal enzyme. We thank Andrea Vasella and Robert Stick for some of the compounds used in the screen. This work is based upon research conducted at the Cornell High Energy Synchrotron Source (CHESS), which is supported by the National Science Foundation under Award DMR-0225180, using the Macromolecular Diffraction at CHESS (MacCHESS) facility, which is supported by award RR-01646 from the National Institutes of Health, through its National Center for Research Resources.

REFERENCES

1. Henrissat, B. (1991) A classification of glycosyl hydrolases based on amino-acid sequence similarities. *Biochem. J. 280*, 309–316.
2. Broquist, H. P. (1985) The indolizidine alkaloids, slaframine and swainsonine: Contaminants in animal forages. *Annu. Rev. Nutr. 5*, 391–409.
3. Tulsiani, D. R., Broquist, H. P., James, L. F., and Touster, O. (1988) Production of hybrid glycoproteins and accumulation of oligosaccharides in the brain of sheep and pigs administered swainsonine or locoweed. *Arch. Biochem. Biophys. 264*, 607–617.
4. Bernacki, R. J., Niedbala, M. J., and Korytnyk, W. (1985) Glycosidases in cancer and invasion. *Cancer Metastasis Rev. 4*, 81–101.
5. Dennis, J. W., Granovsky, M., and Warren, C. E. (1999) Glycoprotein glycosylation and cancer progression. *Biochim. Biophys. Acta 1473*, 21–34.
6. Dube, D. H., and Bertozzi, C. R. (2005) Glycans in cancer and inflammation. Potential for therapeutics and diagnostics. *Nat. Rev. Drug Discovery 4*, 477–488.
7. Hakomori, S. (2002) Glycosylation defining cancer malignancy: new wine in an old bottle. *Proc. Nat. Acad. Sci. U.S.A. 99*, 10231–10233.
8. Goss, P. E., Reid, C. L., Bailey, D., and Dennis, J. W. (1997) Phase IB clinical trial of the oligosaccharide processing inhibitor swainsonine in patients with advanced malignancies. *Clin. Cancer Res. 3*, 1077–1086.
9. Kumar, N. S., Kuntz, D. A., Wen, X., Pinto, B. M., and Rose, D. R. (2008) Binding of sulfonium-ion analogues of di-*epi*-swainsonine and 8-*epi*-lentiginosine to *Drosophila* Golgi α-mannosidase II: The role of water in inhibitor binding. *Proteins. 71*, 1484–1496.
10. Zhong, W., Kuntz, D. A., Ember, B., Singh, H., Moremen, K. W., Rose, D. R., and Boons, G.-J. (2008) Probing the substrate specificity of Golgi α-mannosidase II using synthetic oligosaccharides and a catalytic nucleophile mutant. *J. Am. Chem. Soc. 130*, 8975–8983.
11. Jones, G., Willett, P., Glen, R. C., Leach, A. R., and Taylor, R. (1997) Development and validation of a genetic algorithm for flexible docking. *J. Mol. Biol. 267*, 727–748.
12. Englebienne, P., Fiaux, H., Kuntz, D. A., Corbeil, C. R., Gerber-Lemaire, S., Rose, D. R., and Moitessier, N. (2007) Evaluation of docking programs for predicting binding of Golgi α-mannosidase II inhibitors: a comparison with crystallography. *Proteins 69*, 160–176.
13. Caines, M. E., Hancock, S. M., Tarling, C. A., Wrodnigg, T. M., Stick, R. V., Stütz, A. E., Vasella, A., Withers, S. G., and Strynadka, N. C. (2007) The structural basis of glycosidase inhibition by five-membered iminocyclitols: the clan a glycoside hydrolase endoglycoceramidase as a model system. *Angew. Chem., Int. Ed. 46*, 4474–4476.
14. van den Elsen, J. M., Kuntz, D. A., and Rose, D. R. (2001) Structure of Golgi α-mannosidase II: a target for inhibition of growth and metastasis of cancer cells. *EMBO J. 20*, 3008–3017.
15. Zechel, D. L. (2001) Phd thesis, *University of British Columbia*.
16. Otwinowski, Z., and Minor, W. (1997) Processing of X-ray diffraction data collected in oscillation mode. *Methods Enzymol. 276*, 307–326.
17. Collaborative Computational Project, Number 4. (1994). The CCP4 suite: programs for protein crystallography. *Acta Crystallogr. D50*, 760−763.
18. Brunger, A. T., Adams, P. D., Clore, G. M., Delano, W. L., Gros, P., Grosse-Kunstleve, R. W., Jiang, J. S., Kuszewski, J., Nilges, M., Pannu, N. S., Read, R. J., Rice, L. M., Simonson, T., and Warren, G. L. (1998) Crystallography and NMR system: a new software suite for macromolecular structure determination. *Acta Crystallogr. D54*, 905–921.
19. Lamzin, V. S., Perrakis, A., and Wilson, K. S. (2001) The ARP/WARP suite for automated construction and refinement of protein models, in *Int. Tables for Crystallography. Vol. F: Crystallography of biological macromolecules* (Rossmann, M. G., and Arnold, E., Eds.) pp 720−722, Kluwer Academic Publishers, Dordrecht, The Netherlands.
20. Emsley, P., and Cowtan, K. (2004) Coot: model-building tools for molecular graphics. *Acta Crystallogr. D60*, 2126–2132.
21. Murshudov, G. N., Vagin, A. A., and Dodson, E. J. (1997) Refinement of macromolecular structures by the maximum-likelihood method. *Acta Crystallogr. D53*, 240–255.
22. Sheldrick, G. M., and Schneider, T. R. (1997) SHELX: high resolution refinement. *Methods Enzymol. 277*, 319–343.
23. Krissinel, E., and Henrick, K. (2004) Secondary-structure matching (SSM), a new tool for fast protein structure alignment in three dimensions. *Acta Crystallogr. D60*, 2256–2268.
24. Berman, H. M., Westbrook, J., Feng, Z., Gilliland, G., Bhat, G., Weissig, H., Shindyalov, I. N., and Bourne, P. E. (2000) The Protein Data Bank. *Nucleic Acids Res. 28*, 235–242.
25. Shah, N., Kuntz, D. A., and Rose, D. R. (2003) Comparative structural analysis of the binding of the inhibitor kifunensine to Class I and Class II α-mannosidases. *Biochemistry 42*, 13812–13816.
26. Vasella, A., Davies, G. J., and Bohm, M. (2002) Glycosidase mechanisms. *Curr. Opin. Chem. Biol. 5*, 619–629.
27. Money, V. A., Smith, N. L., Scaffidi, A., Stick, R. V., Gilbert, H. J., and Davies, G. J. (2006) Substrate distortion by a lichenase highlights the different conformational itineraries harnessed by related glycoside hydrolases. *Angew. Chem., Int. Ed. 45*, 5136–5140.
28. Dorfmueller, H. C., Borodkin, V. S., Schimpl, M., Shepherd, S. M., Shpiro, N. A., and van Aalten, D. M. (2006) GlcNAcstatin: a picomolar, selective O-GlcNAcase inhibitor that modulates intracellular O-glcNAcylation levels. *J. Am. Chem. Soc. 128*, 16484–16485.
29. Granier, T., Panday, N., and Vasella, A. (1997) Structure-activity relations for imidazo-pyridine-type inhibitors of β-D-glucosidases. *Helv. Chim. Acta 80*, 979–987.
30. Panday, N., Canac, Y., and Vasella, A. (2000) Very strong inhibition of β-glucosidases by *C*(2)-substituted tetrahydroimidazopyridines. *Helv. Chim. Acta 83*, 58–79.
31. Numao, S., Kuntz, D. A., Withers, S. G., and Rose, D. R. (2003) Insights into the mechanism of *Drosophila melanogaster* Golgi α-mannosidase through the structural analysis of covalent reaction intermediates. *J. Biol. Chem. 278*, 48074–48083.
32. Tailford, L. E., Offen, W. A., Smith, N. L., Dumon, C., Morland, C., Gratien, J., Heck, M.-P., Stick, R. V., Blériot, Y., Vasella, A., Gilbert, H. J., and Davies, G. J. (2008) Structural and biochemical evidence for a boat-like transition state in β-mannosidases. *Nat. Chem. Biol. 5*, 306–312.
33. Liu, H., Liangm, X., Søhoel, H., Bülow, A., and Bols, M. (2001) Noeuromycin, a glycosyl cation mimic that strongly inhibitis glycosidases. *J. Am. Chem. Soc. 123*, 5116–5117.
34. Jespersen, T. M., Dong, W., Sierks, M. R., Skrydstrup, T., Lundt, I., and Bols, M. (1994) Isofagomine, a potent, new glycosidase inhibitor. *Angew. Chem., Int. Ed. Engl. 33*, 1778–1779.
35. Fuhrmann, U., Bause, E., Legler, G., and Ploegh, H. (1984)) Novel mannosidase inhibitor blocking conversion of high mannose to complex oligosaccharides. *Nature 307*, 755–758.
36. Kuntz, D. A., Liu, H., Bols, M., and Rose, D. R. (2006) The role of the active site Zn in the catalytic mechanism of the GH38 Golgi α-mannosidase II: implications from noeuromycin inhibition. *Biocatal. Biotransform. 24*, 55–61.
37. Gloster, T. M., Roberts, S., Perugino, G., Rossi, M., Moracci, M., Panday, N., Terinek, M., Vasella, A., and Davies, G. J. (2006) Structural, kinetic and thermodynamic analysis of glucoimidazole-derived glycosidase inhibitors. *Biochemistry 45*, 11879–11884.
38. Ogawa, S., Ashiura, M., Uchida, C., Watanabe, S., Yamazaki, C., Yamagishi, K., and Inokuchi, J. (1996) Synthesis of potent β-D-glucocerebrosidase inhibitors: N-alkyl-β-valienamines. *Bioorg. Med. Chem. Lett. 6*, 929–932.
39. Lin, H., Sugimoto, Y., Ohsaki, Y., Ninomiya, H., Oka, A., Taniguchi, M., Ida, H., Eto, Y., Ogawa, S., Matsuzaki, Y., Sawa, M., Inoue, T.,

Higaki, K., Nanba, E., Ohno, K., and Suzuki, Y. (2004) N-octyl-β-valienamine up-regulates activity of F213I mutant β-glucosidase in cultured cells: a potential chemical chaperone therapy for Gaucher disease. *Biochim. Biophys. Acta 1689*, 219–228.

40. Lei, K., Ninomiya, H., Suzuki, M., Inoue, T., Sawa, M., Iida, M., Ida, H., Eto, Y., Ogawa, S., Ohno, K., and Suzuki, Y. (2007) Enzyme enhancement activity of N-octyl-β-valienamine on β-glucosidase mutants associated with Gaucher disease. *Biochim. Biophys. Acta 1772*, 587–596.
41. Li, C., Begum, A., Numao, S., Park, K. H., Withers, S. G., and Brayer, G. D. (2005) Acarbose rearrangement mechanism implied by the kinetic and structural analysis of human pancreatic alpha-amylase in complex with analogues and their elongated counterparts. *Biochemistry 44*, 3347–3357.
42. Scaffidi, A., Stubbs, K. A., Dennis, R. J., Taylor, E. J., Davies, G. J., Vocadlo, D. J., and Stick, R. V. (2007) A 1-acetamido derivative of 6-epi-valienamine: an inhibitor of a diverse group of β-N-acetylglucosaminidases. *Org. Biomol. Chem. 5*, 3013–3019.
43. Hoos, R., Naughton, A. B., Thiel, W., Vasella, A., Weber, W., Rupitz, K., and Withers, S. G. (1993) D-Gluconhydroximino-1,5-lactam and related N-arylcarbamates. Theoretical calculations, structure, synthesis, and inhibitory effect on β-glucosidases. *Helv. Chim. Acta 76*, 2666–2686.
44. Gloster, T. M., Meloncelli, P., Stick, R. V., Zechel, D., Vasella, A., and Davies, G. J. (2007) Glycosidase inhibition: an assessment of the binding of 18 putative transition-state mimics. *J. Am. Chem. Soc. 129*, 2345–2354.
45. Burmeister, W. P., Cottaz, S., Rollin, P., Vasella, A., and Henrissat, B. (2000) High resolution X-ray crystallography shows that ascorbate is a cofactor for myrosinase and substitutes for the function of the catalytic base. *J. Biol. Chem. 275*, 39385–39393.
46. Elbein, A. D., Tropea, J. E., Mitchell, M., and Kaushal, G. P. (1990) Kifunensine, a potent inhibitor of the glycoprotein processing mannosidase I. *J. Biol. Chem. 265*, 15599–15605.
47. Vallee, F., Karaveg, K., Herscovics, A., Moremen, K. W., and Howell, P. L. (2000) Structural basis for catalysis and inhibition of N-glycan processing class I α 1,2-mannosidases. *J. Biol. Chem. 275*, 41287–41298.
48. Wicki, J., Williams, S. J., and Withers, S. G. (2007) Transition-state mimicry by glycosidase inhibitors: A critical kinetic analysis. *J. Am. Chem. Soc. 129*, 4530–4531.
49. Hrmova, M., Stretltsov, V. A., Smith, B. J., Vasella, A., Varghese, J. N., and Fincher, G. B. (2005) Structural rationale for low-nanomolar binding of transition state mimics to a Family GH3 β-D-glucan glucohydrolase from barley. *Biochemistry 44*, 16529–16539.
50. Gloster, T. M., Macdonald, J. M., Tarling, C. A., Stick, R. V., Withers, S. G., and Davies, G. J. (2004) Structural, thermodynamic, and kinetic analyses of tetrahydrooxazine-derived inhibitors bound to β-glucosidases. *J. Biol. Chem. 279*, 49236–49242.
51. Gartenmann Dickson, L., Emmanuel, L., and Reymond, J.-L. (2004) Structure-activity relationships in aminocyclopentitol glycosidase inhibitors. *Org. Biomol. Chem. 2*, 1217–1226.
52. Li, B., Kawatkar, S. P., George, S., Strachan, H., Woods, R. J., Siriwardena, A., Moremen, K. W., and Boons, G.-J. (2004) Inhibition of Golgi mannosidase II with mannostatin A analogues: synthesis, biological evaluation, and structure-activity relationship studies. *ChemBioChem 5*, 1220–1227.
53. Kawatkar, S. P., Kuntz, D. A., Woods, R. J., Rose, D. R., and Boons, G.-J. (2006) Structural basis of the inhibition of Golgi α-mannosidase II by mannostatin A and the role of the thiomethyl moiety in ligand-protein interactions. *J. Am. Chem. Soc. 128*, 8310–8319.
54. Shah, N., Kuntz, D. A., and Rose, D. R. (2008) Golgi α-mannosidase II cleaves two sugars sequentially in the same catalytic site. *Proc. Natl. Acad. Sci. U.S.A. 105*, 9570–9575.

BI8010785